Resonantly loaded apertures for high-resolution near field surface imaging

Malyuskin, O., & Fusco, V. (2015). Resonantly loaded apertures for high-resolution near field surface imaging. *IET Science, Measurement and Technology*, *9*(7), 783-791. https://doi.org/10.1049/iet-smt.2014.0337

Published in:
IET Science, Measurement and Technology

Document Version:
Peer reviewed version

Resonantly loaded apertures for high-resolution near field surface imaging

Oleksandr Malyuskin and Vincent Fusco

The Institute of Electronics, Communications and Information Technology
Queen's University Belfast, Queen's Rd, Belfast, BT3 9DT, UK
E-mail: o.malyuskin@qub.ac.uk; v.fusco@ecit.qub.ac.uk

Abstract

A novel type of microwave probes based on the loaded aperture geometry has been proposed and experimentally evaluated for dielectrics characterization and high-resolution near field imaging. Experimental results demonstrate the possibility of very accurate microwave spectroscopic characterization of thin lossy dielectric samples and biological materials containing water. High resolution images of the subwavelength lossy dielectric strips and wet and dry leaves have been obtained with amplitude contrast around 10-20dB and spatial resolution better than one tenth of a wavelength in the near field zone. A microwave imaging scenario for the early-stage skin cancer identification based on the artificial dielectric model has also been explored. This model study shows that the typical resolution of an artificial malignant tumour with a characteristic size of one tenth of a wavelength can be discriminated with at least 6dB amplitude and 50 degrees phase contrast from the artificial healthy skin and with more than 3dB contrast from a benign lesion of the same size. It has also been demonstrated that the proposed device can efficiently deliver microwave energy to very small, subwavelength, focal areas which is highly sought in the microwave hyperthermia applications.

1. Introduction

Radiofrequency and microwave radiation has been widely used in medical diagnostic and therapy for several decades [1]. Particularly, microwaves are used to treat arrhythmia and perform various types of ablation in cardiology and cancer therapy [2], [3]. They are also employed to manage the patient's pain and to treat chronic medical conditions [4].

Another area of microwave medical applications is related to non-invasive measurements of dielectric properties of biological materials. The knowledge of dielectric permittivity of a biological sample or dielectric contrast between biological tissues is important for the detection and treatment of melanoma skin cancer [5], real-time assessment of the glucose level for diabetes monitoring [6], electrical impedance biopsy [7], etc.

Several types of microwave probes have been developed for the material surface characterization. The most common and widely used probe is an open-ended coaxial cable probe [2],[7]-[12]. Another class of probes is represented by the microstrip transmission lines or conductive patch elements printed on dielectric substrates [6], [13], [14]. A dipole antenna [15] and the open-ended waveguide probes [16], [17] were also proposed previously.

The microwave probes of considered types possess different imaging characteristics and operational frequency bandwidth which define their area of application. An open-ended coaxial probe forms a tight electric field intensity focal spot in the near field zone with the dominant electric field component parallel to the coaxial cable axis. This *E*-field is very well collimated in the immediate vicinity of the coaxial open end, $\lambda/100$ - $\lambda/6$, λ is a wavelength of radiation, and diverges very fast as the distance from the probe increases. Consequently the high-resolution imaging distance of an open-ended coaxial is limited by approximately $\lambda/6$ distance. The advantage of the probe is in its wide operational frequency range [7] and simple design scalable across the frequency ranges. The major drawback of the open-ended coaxial probe is its very inefficient coupling to the material sample arising from a high reflection level from the coaxial open end [7]. This significantly limits

the measurements' signal-to-noise ratio and makes efficient microwave energy delivery to the illuminated spot very difficult.

Printed microstrips and patch antennas have been successfully used for non-destructive characterization of biological samples by measuring the resonance frequency shift of the antenna in the presence of the biological substance [6], [13], [14]. The imaging distance of these sensors is limited to the immediate proximity ($< \lambda/50$) due to the presence of dielectric substrate which leads to the electromagnetic field localisation near the substrate surface. Also, in general, subwavelength high-resolution imaging is not possible due to the lack of near field focusing characteristics consequently only spatially averaged properties of the material can be measured.

Other imaging setups such as a dipole antenna parallel to the surface of the sample [15] and an open-ended waveguide probe [16], [17] exhibit major limitations due to their large spatial near field electrical footprint leading to low-resolution imaging properties. Particularly, the characteristic imaging resolution of an open-ended waveguide is intrinsically diffraction limited and exceeds half-wavelength. A half-wavelength dipole probe enables one-dimensional subwavelength resolution in the range orthogonal to its length, however the dipole near field pattern is rapidly diverging with increasing imaging distance and typical resolution contrast is very low (~1-2dB) even at imaging distances less than $\lambda/10$ [18].

Recently the authors of the present paper proposed a novel class of probes comprised of small or non-resonant apertures loaded with resonant inserts [18]-[20]. These resonantly loaded apertures allow significant enhancement of the electric and magnetic near fields as well as deep subwavelength field collimation in the near field zone. Major advantages of this type of probes are: (*i*) they enable very high imaging resolution over the entire near field imaging distances range ($\lambda/100$- $\lambda/4$), (*ii*) they can efficiently operate with low level of microwave radiation power and, (*iii*) they offer the possibility of real-time high-resolution imaging [20]. Previously, these probes have been successfully applied to subwavelength imaging of dielectric and metal targets [19], [20].

In this paper we give the first reported discussion of the sensitivity and near field imaging resolution of the resonantly loaded aperture probes to small planar dielectric structures, particularly, lossy dielectric strips and patches and biological samples with different water content.

Imaging of water content difference in material is important in particular for skin cancer identification by the microwave and millimetre-wave sensors [21], [22]. Experimental data show that malignant skin tissue contains substantially higher amount of water (around 20%) than the normal skin [23], while benign lesions typically tend to be few percent drier than the healthy skin [24]. From the microwave reflectometry point of view different water content in imaged material leads to variation in the microwave signal reflection and absorption which can be detected by the resonance reflectometer with high accuracy. To study a possibility of early-stage skin cancer detection by resonance microwave probes, an artificial skin model has been developed using lossy dielectric Eccosorb materials [25] that can model microwave properties of the healthy skin, malignant tumours and benign lesions. The model studies show that the typical resolution of an artificial malignant tumour with a characteristic size of one tenth of a wavelength can be discriminated with at least 6dB amplitude and 50 degrees phase contrast from the dielectric sheet modelling healthy skin and with more than 3dB contrast from an artificial benign lesion of the same size.

It should be noted that even though this paper is focused on differential imaging where the dielectric contrast or resonance frequency shift between the samples is of primary interest, the proposed technique can be used for absolute permittivity measurements using resonance frequency perturbation analysis developed in [26]-[28]. This possibility will be studied in future work.

Finally, the unique ability of efficient microwave energy delivery to very small spatial area by resonantly loaded apertures is demonstrated. It is believed that the proposed class of probes could assist in the development of new applications in biological surface characterization and imaging and microwave hyperthermia where highly collimated near field beam properties play a key role.

2. Loaded aperture probe construction and principle of operation

The loaded aperture imaging device (probe) can be constructed using a metal screen or screens with arbitrary shaped apertures loaded with planar or quasi-planar conductive inserts [20]. The loaded aperture is backed by a metal cavity for efficient microwave excitation and reflected signal reception, Fig.1(a),(b).

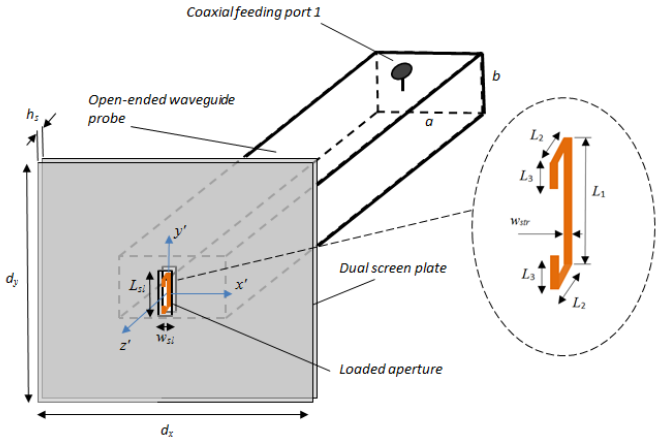

(a)

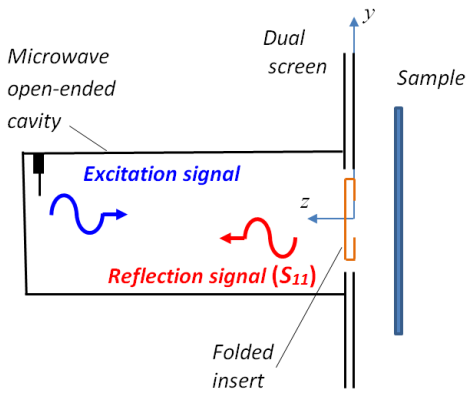

(b)

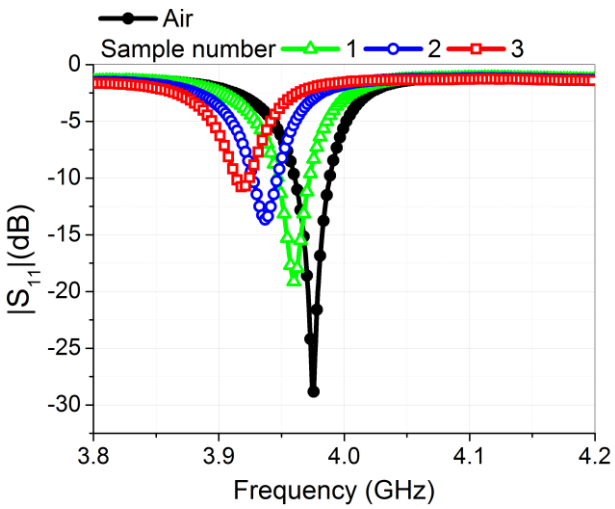

(c)

Fig. 1. Loaded aperture probe construction, 3D view (a) and side view (b) and measured frequency spectrum of the reflected signal for the standalone probe in air (black line with dot markers) and in the presence of different dielectric samples positioned at 3mm standoff distance from the aperture (c). The material samples are thin lossy dielectric strips of 30mm length, 5mm width and 0.5mm and 1mm thickness. The sample 1 corresponds to the Eccosorb [25] material BSR-U, sample 2 – to the material FGM-U40, sample 3- to the material GDS-U, more details are given in Section 3.

When the probe is positioned in free space (air) with no imaged sample located close to the aperture, a resonance dip in reflection (S_{11} parameter) occurs, Fig.1(c), black line with dot markers, meaning that there is a highly enhanced transmitted electric field in the vicinity of the aperture, Fig.2. When a material sample is brought in the high intensity microwave field area, electric polarization

of the sample leads to the reflection resonance frequency shift, Fig.1(c), determined by the sample dielectric permittivity and shape. Thus from the resonance frequency shift the properties of the sample can be inferred. Furthermore since the near field focal area is substantially confined in space, Fig.2, with full width at half-maximum (FWHM) ~0.1λ – 0.2λ, imaging of the material sample spatial properties with resolution ~0.1λ – 0.2λ is also feasible [20].

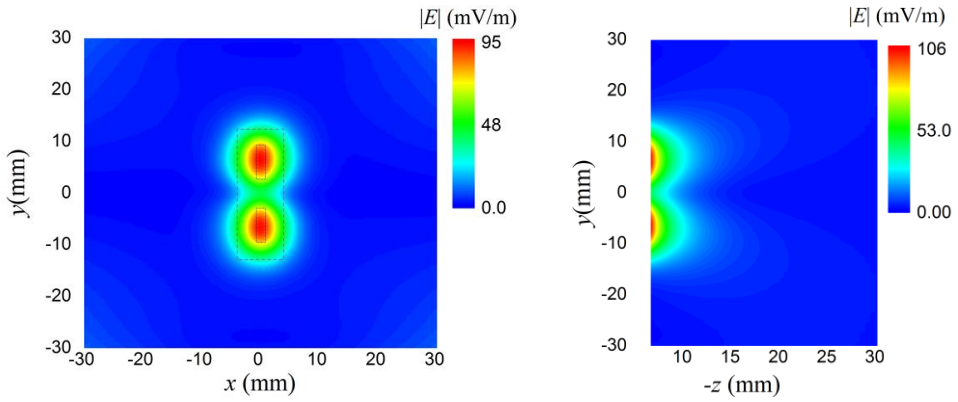

(a) (b)

Fig. 2. Simulated (FEKO) electric near field intensity in the vicinity of folded strip loaded aperture in the horizontal (xy) plane (a) and vertical plane (yz) (b) at 4GHz. The spatial dimensions of the probe shown in Fig 1(a) designed for the 4GHz range are d_x=d_y=66mm, h_s =3mm, L_{sl}=25mm, w_{sl} =7mm, L_1=18mm, L_2=3mm, L_3=6mm, w_{str}=2mm.

The high-quality resonance transmission in loaded apertures occurs due to significant electric charge separation along the insert. The slot boundaries act as a subwavelength resonator, enhancing and collimating the *E*-field [20].

TABLE I. **FWHM (IN WAVELENGTH) OF THE LOADED APERTURE NEAR FIELD**

z′/ λ	**|E|**	**|H|**
0.01	0.04	0.11
0.05	0.11	0.14
0.1	0.18	0.19
0.15	0.23	0.26
0.2	0.30	0.40
0.25	0.42	0.53

In the present paper we demonstrate the possibility of both spectral characterization and spatial differential imaging of lossy dielectric materials using a folded strip loaded aperture probe shown in Fig.1(a). The resonance frequency response of the standalone probe in air is shown in Fig.1(c), black line with dot markers. The near field spatial properties are characterized by the near field pattern FWHM which are summarised in Table I as a function of imaging stand-off distance z'/λ. The FWHM defines the characteristic resolution of the probe, whose median value is around 0.1λ in the range of stand-off distances 0.01λ -0.15λ.

3. Lossy dielectrics characterization and subwavelength imaging

In order to demonstrate the subwavelength imaging resolution and spectral response of the folded insert loaded aperture probe a sample consisting of lossy dielectric strips with known parameters has been made, Fig.3(a). The sample consists of three strips (arranged in two rows) of lossy artificial dielectric absorber material Emerson and Cuming Eccosorb [25] with specifications BSR-U, FGM-U and GDS-U. These specifications have different microwave attenuation level at 4GHz: 15dB/cm for GDS-U, 17.5dB/cm for FGM-U, and 21dB/cm for BSR-U. Additionally the samples differ by thickness: the thickness of the BSR sample is 0.5 mm, while the FGM and GDS dielectric strips are 1mm thick. The real part of the permittivity of these dielectrics is around 10, $\tan\delta$~0.2-0.4. The strips lay on the 1cm thick Rohacell foam substrate with permittivity 1.07.

The imaging set-up is shown in Fig. 3(b), the loaded aperture is excited by the open-ended waveguide section with dominant TE_{10} mode generated via coaxial port feeding. The probe resonates around 4GHz with wavelength λ=75mm. The probe was positioned on the planar NSI near field system scanner [29], while the sample is held in vertical position on the wooden frame such that the imaging distance remains the same during the scan in the x-y plane.

The measured spectral response of the dielectric strips is shown in Fig.1(c) where sample 1 denotes BSR dielectric strip, sample 2 stands for FGM strip and sample 3 denotes GDS dielectric strip. For this measurement the loaded aperture has been positioned at 3mm distance from the surface of each strip. It can be seen that the probe spectral response strongly depends on the permittivity of the dielectric strips – the highest level of reflection is achieved for the GDS dielectric strip (sample

3) with lowest microwave loss.

The raw spatial images of the dielectric samples have been obtained for two frequencies, 3.947GHz and 3.965GHz around the probe resonance at 5mm imaging distance (middle of the imaging range 1-10mm), Fig.4. This resonance frequency choice corresponds to the reflection resonance of FGM material, and probe in air, Fig.1(c).

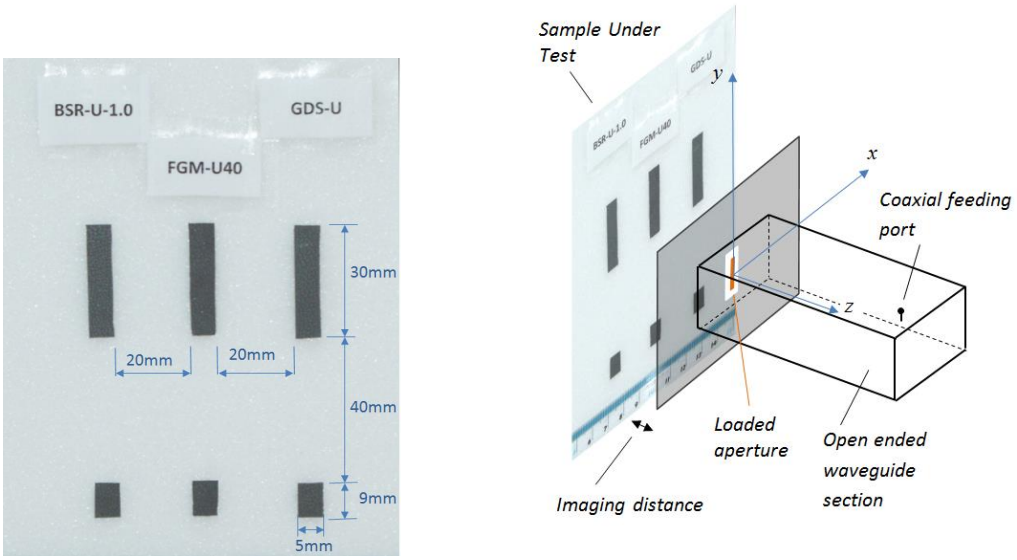

(a) (b)

Fig. 3. A sample consisting of lossy dielectric strips (a) and imaging setup geometry (b), loaded aperture is shown schematically for clarity.

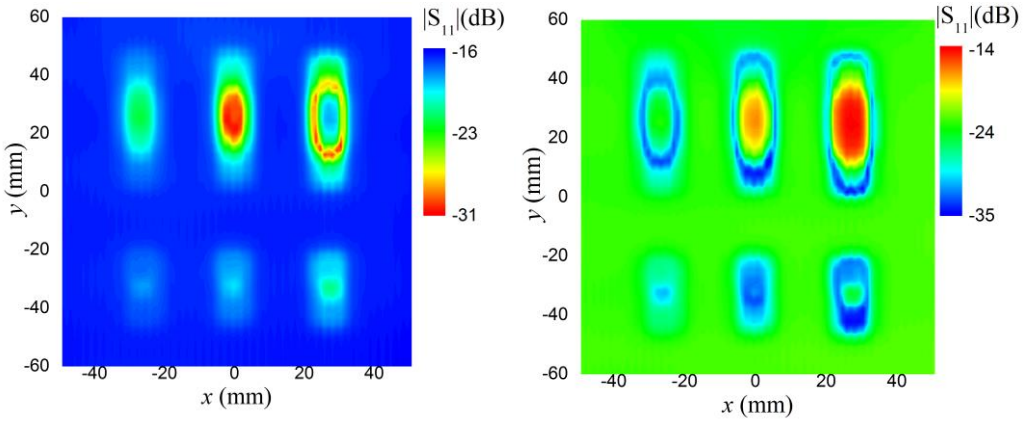

(a) (b)

Fig. 4. Dielectric strips reflection images obtained at 3.947GHz (a) and 3.965GHz (b). Imaging distance is 5mm. Imaging step is 1.25mm in both x and y directions.

At 4 GHz the dimensions (length x width x thickness) of the longer strips (top row) are 0.4λ x0.07λ x0.01λ and the dimensions of the shorter strips (bottom row) are 0.07λx 0.07λx0.01λ. It can be seen from Fig.4 that not only the shape of the longer strips but also the short strips having deep subwavelength dimensions (~0.07λ x 0.07λ) are clearly imaged. The top strips images are obtained with high resolution contrast (~ 10dB) while in the case of short strips the resolution contrast is significantly lower (1-3dB). Due to the fact that near field coupling (resonance frequency) of the probe to the dielectric sample depends on their relative position, imaging at different frequencies would allow clear dielectric pattern shape reconstruction (e.g. see Fig.4 where the GDS dielectric strip rim is imaged with high-resolution). However, as follows from the results presented in Fig.4, microwave loss leads to image blurring (e.g. the image of FGM dielectric strip). The BSR dielectric strip generates the weakest reflection image due to (*i*) smaller thickness and (*ii*) higher level of absorption in BSR material which results in lower level of near field coupling.

It should be noted that for larger stand-off distances (more than 5mm) the imaging resolution degrades proportionally to the *E*- Field FWHM given by the Table I, middle column. At the same time if the probe is positioned too closely to the surface of lossy dielectric (less than 2mm) high microwave loss in material can substantially affect the probe resonance quality thus resolution contrast can degrade. This effect is not discussed here in detail for the brevity's sake and will be explored elsewhere in future.

4. Artificial dielectric skin model for early stage skin cancer imaging scenario

Biomedical studies show that malignant melanoma typically has 10-20% higher water content than the healthy skin tissue, while benign lesions are typically drier by several percent than healthy skin [23], [24]. Difference in the material water content results in different electromagnetic signal reflection and absorption or, equivalently, near field coupling which can be detected by the reflectometer. Previous microwave and millimetre-wave imaging studies [21],[22] demonstrated the possibility of EM discrimination between the healthy and malignant tissue, however the measured

reflection signal contrast appeared to be prohibitively low (1-3dB) due to inefficient coupling of open-ended waveguide and open-ended coaxial probes to tissue.

In this paper an artificial dielectric skin model is developed using three types of Eccosorb dielectric materials [25] – GDS-U (corresponds to benign lesions), FGM-U (healthy skin) and BSR-U (malignant tumour). The equivalence of the proposed thin dielectric sheet model to the microwave properties of the skin cancer tissue is based on different microwave attenuation in the GDS, FGM and BSR materials, Fig. 5, which represents water content difference in benign, healthy and malignant skin tissue. To further analyse the relevance of the proposed dielectric model to the skin cancer identification scenario, we show on the same plot in Fig.5 the microwave attenuation of dry and wet human skin obtained from the experimental data [30], [31] . It has been shown previously [21], [22] that the microwave reflection contrast between the malignant tumour and healthy skin and dry and wet skin is approximately the same. Therefore microwave attenuation contrast between the dry and wet skin, Fig.5, can serve as a qualitative estimation for the microwave contrast between the melanoma and normal skin tissue. From Fig. 5 one can see that the microwave attenuation in human skin is an order of magnitude higher than the attenuation in the Eccosorb materials, however the attenuation difference is approximately the same ~5dB in the considered frequency range 1-10GHz. It should be stressed that the differential reflection image arises as a result of microwave contrast, but not the absolute value of the sample permittivity parameters. It is also interesting to note that the attenuation contrast between the dry and wet skin is around 1.5 times higher than the contrast between the FGM-U and BSR-U materials therefore imaging resolution should generally be better for the in-vivo imaging scenario.

The resolution of the loaded aperture probe is assessed in terms of a wavelength, so the probe dimensions can be scaled down to achieve absolute spatial resolution of 1mm or smaller. The operation frequency for this resolution to be obtained should be around 30GHz.

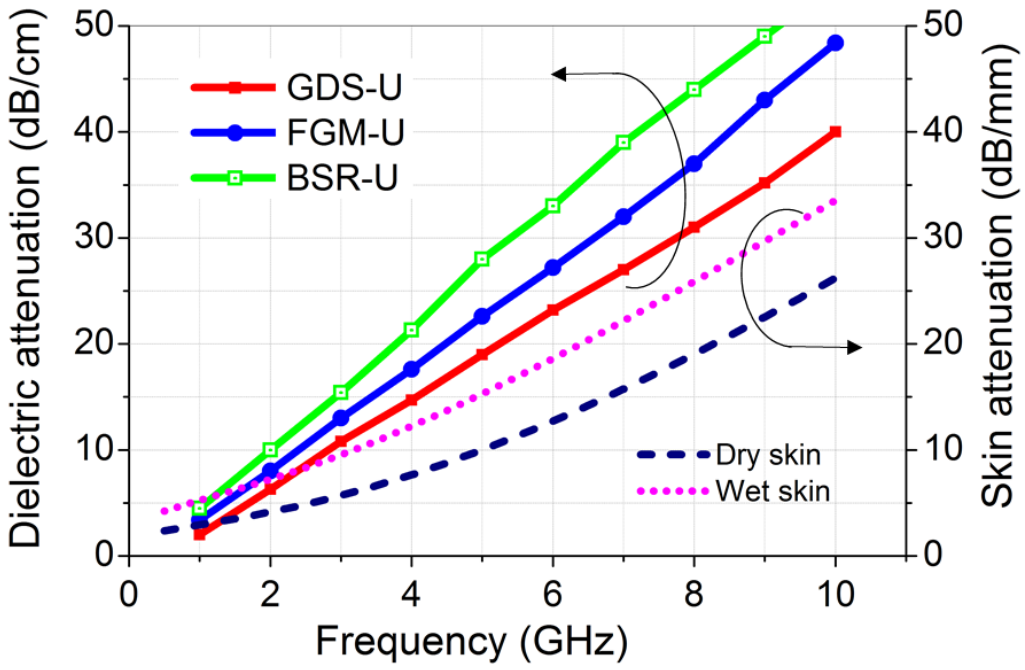

Fig.5. Typical attenuation of 1mm thick dielectric sheets of Eccosorb materials GDS-U, FGM-U and BSR-U [25] and dry and wet skin [30], [31].

The spatial pattern of the skin cancer model, Fig.6(a), is designed to represent skin cancer development at the early stages [32] when only small, node-like tumours occur. In addition, two patches are added to model the benign lesions. In Fig.6(a), the BSR patches (highest microwave loss from three materials) model melanoma regions, the GDS patches (lowest microwave loss) model benign lesions and the healthy skin is modelled by the FGM-U material sheet (with intermediate microwave loss). The thickness of all material layers is 1mm. The characteristic size of the patches varies from ~5mm (λ/15) to 10mm (λ/7.5). It can be seen that the reflection contrast between two large BSR patches (melanoma) on top of the sheet and FGM-U layer is more than 10dB. At the same time, the reflection contrast between the large GDS-U (benign lesion) patch and FGM-U substrate is less than 6dB. This indicates the possibility of very accurate melanoma detection and discrimination from the healthy skin and benign lesions in differential reflectometry measurements. The small BSR and GDS patches in the bottom of the structure (encircled with white dotted lines in the reflection image) are less clearly resolved, with contrast ~3dB for BSR and ~1dB for GDS patches respectively. This shows the resolution limits of the proposed resonantly loaded probe capable of imaging lossy inhomogeneities (placed on lossy substrate) of characteristic size only larger than ~0.1λ. It should be

noted that the geometry of the considered skin cancer model does not exactly represent human skin layered structure (skin- subcutaneous fat -muscle) however as experiments show the near field coupling of a resonance probe to a layered lossy structure is dominantly determined by the properties of a high permittivity top layer (skin) and does not depend appreciably on the properties of the bottom layers of lower permittivity (subcutaneous fat).

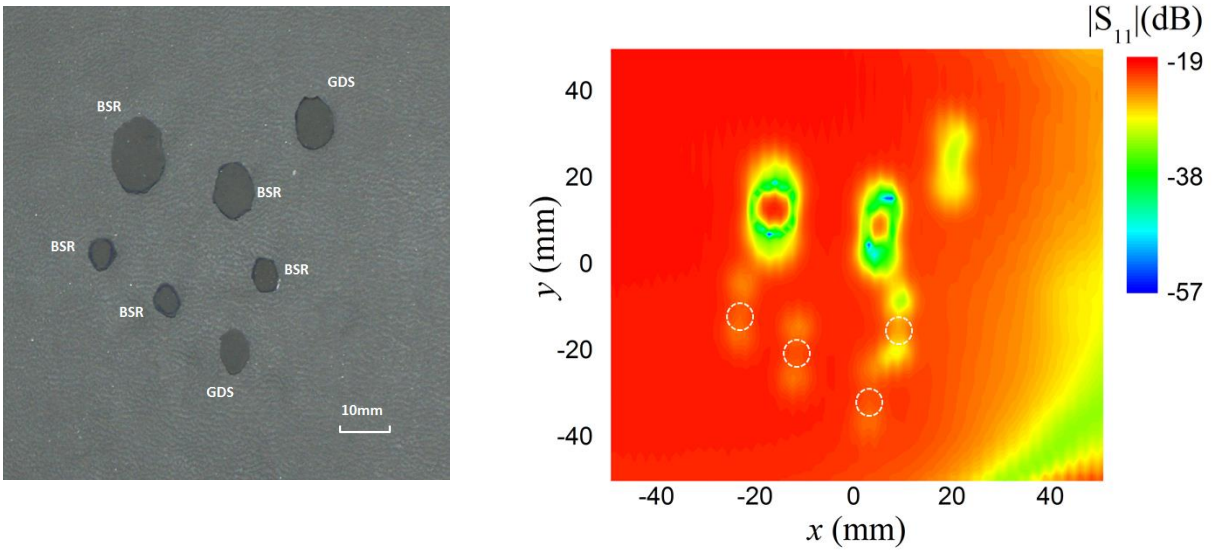

(a) (b)

Fig.6. (a) Artificial dielectric skin model consisting of BSR-U (representing melanoma) and GDS-U (benign lesions) dielectric patches on the FGM-U (healthy skin) sheet material; (b) amplitude reflection image. White dotted line circles on the reflection image plot show the positions of four small patches in the bottom of the structure.

5. Imaging of bio-material with different water content

To illustrate the probe capabilities for microwave imaging of biomaterials containing water a sample consisting of wet and dry leaves has been prepared, Fig. 7(a). To ensure uniform imaging distance the leaves have been pressed with a thin (few micrometres thick) polymeric film. The resonance responses for the leaves is shown in Fig.7(b) at 5mm imaging distance. It can be seen that the presence of water (dielectric permittivity ~80) leads to significant resonance frequency shift and the reflection amplitude level change. The raw microwave images obtained at 5mm imaging distance at 3.98GHz are shown in Fig.8. It can be seen that the green leaves are imaged with very contrast

(~20dB) and spatial resolution (~5mm). The blue rim around the leaves demonstrates the edge near field coupling mechanism (which is promising for high-contrast shape resolution). The amplitude imaging contrast of dry leaf in the top right corner is reduced (~5dB) as compared to the wet leaves however the presence of blue rim around the dry leaf area indicates the edge near field strong coupling. It is interesting to note that the reflection phase images, Fig.8(b) also demonstrate very high contrast (more than 100 degrees) and spatial resolution (~5mm).

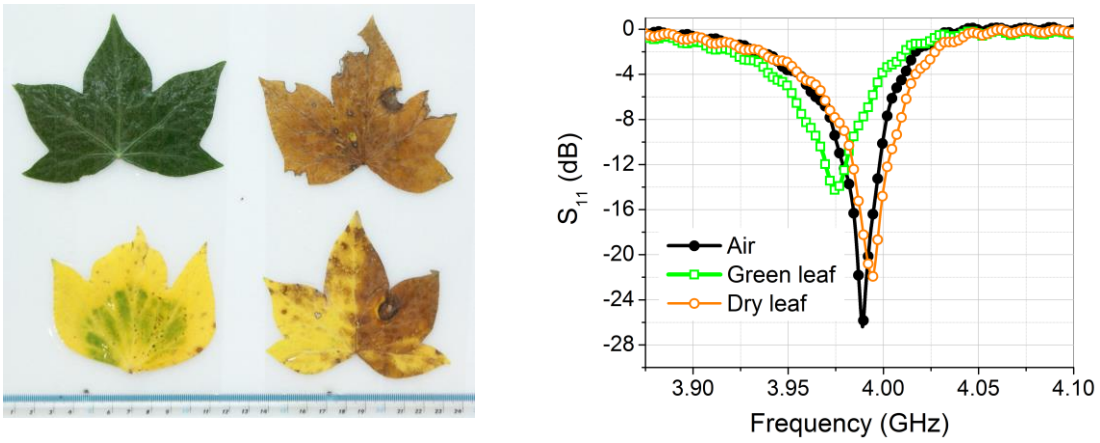

(a) (b)

Fig. 7. Green (wet) and dry leaves sample (a) and spectral response of the leaves (b).

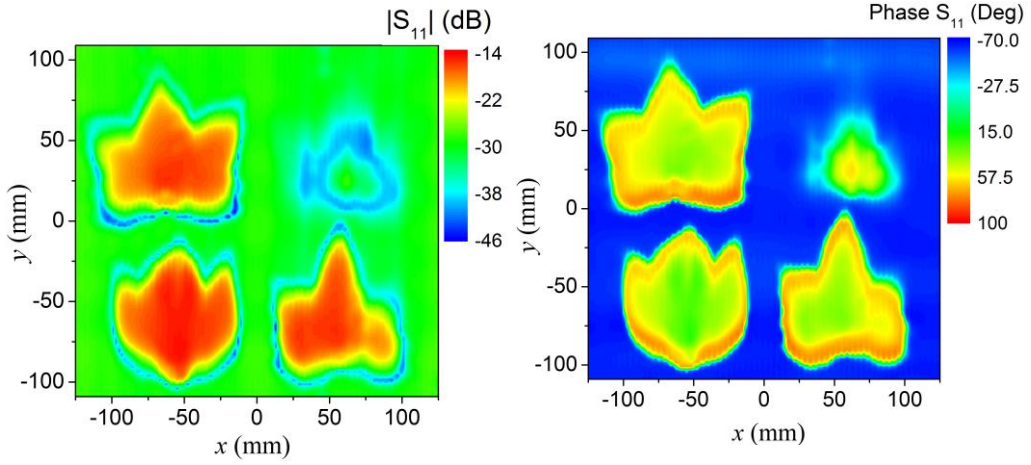

(a) (b)

Fig. 8. Reflection amplitude (a) and phase (b) images at 3.98GHz. Imaging distance is 5mm. Measurement step is 2.5mm in both x and y directions

6. Loaded aperture probe sensitivity to thin dielectric samples

Qualitative analysis of the loaded aperture probe sensitivity to thin dielectric samples dependent on the image setup and sample geometry and dielectric properties is given in this Section.

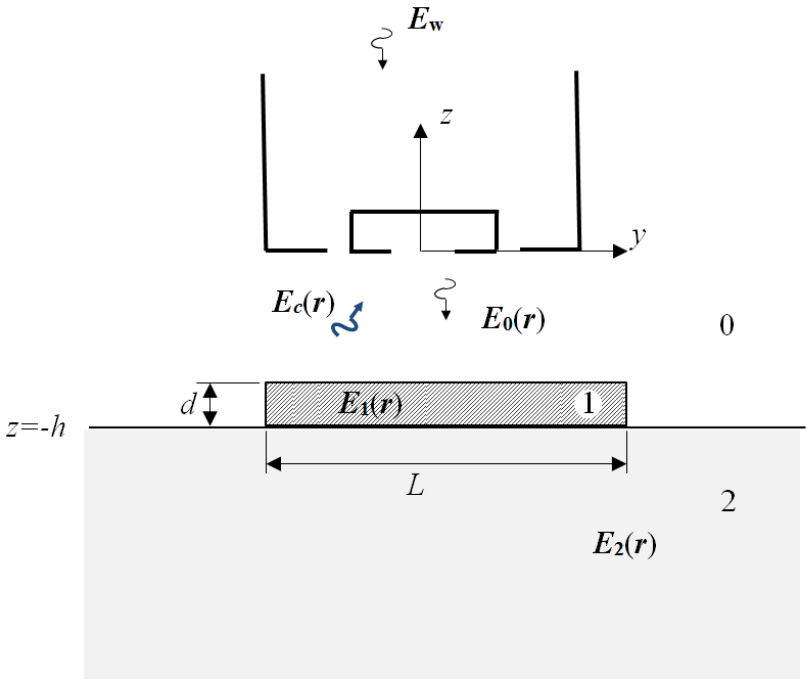

Fig. 9. This dielectric sample imaging geometry, *xy* plane view

The effects of the imaging distance, sample geometry and its dielectric properties and the presence of dielectric substrate (background), Fig.9, are analysed using a quasi-static approximation [31]. In Fig.9 the imaged sample is represented by a thin dielectric strip of length *L*, width *w* and depth *d*, with geometry parameters satisfying the condition $L \sim w >> d$. The relative permittivity of the sample is ε_1, the relative permittivity of dielectric substrate is ε_2.

The loaded aperture is excited by a waveguide mode TE_{10} with electric field $\boldsymbol{E}_w$. In [20] it has been shown that the near field $\boldsymbol{E}_0$ transmitted into the air in region 0, z < 0, represents a dipole field mode with dominant $\sim 1/\boldsymbol{r}^3$ (in quasi-static zone) spatial dependence. This *E*-field causes depolarization of the dielectric with electric current densities $J_{1y}(\boldsymbol{r}_1)$, $J_{2y}(\boldsymbol{r}_2)$

$$J_{1y}(\boldsymbol{r}_1) = -i\omega\varepsilon_0(\varepsilon_1 - 1)\int_{V_1} E_{1y}(\boldsymbol{r}_1')d\boldsymbol{r}_1'$$
$$\approx -i\omega\varepsilon_0 V_1 \frac{(\varepsilon_1 - 1)}{1 + \frac{d}{L}(\varepsilon_1 - 1)} E_{0y}(z_1) \quad (1)$$

$$J_{2y}(\boldsymbol{r}_2) = -i\omega\varepsilon_0(\varepsilon_2 - 1)\int_{V_2} E_{2y}(\boldsymbol{r}_2')d\boldsymbol{r}_2' \quad (2)$$

where only the dominant *y*-components of the fields and polarization currents are taken into account and monochromatic exp (-*i*ωt) time dependence is assumed. In (1) the radius vector $\boldsymbol{r}_1$ is within the volume V_1 of the strip, V_1=*Lwd*, z_1=*d*-*h*. In derivation of the second part of the formula (1) the polarizability of the strip is approximated as the polarizability of a thin elliptical disk in the long axis direction [33]. In (2) the radius vector $\boldsymbol{r}_2$ is within the volume V_2 of the substrate. It should be noted that due to the continuity of the fields tangential components, the field $E_{2y} \approx E_{0y}$ in the thin layer of substrate in the vicinity of the boundary *z* =-*h*. This layer gives the dominant contribution to the dielectric substrate coupling to the probe. The near field coupling of the sample to the probe is due to the electric field $\boldsymbol{E}_c$ excited by the sum of depolarization electric currents (1), (2). In the near field region this field decays proportionally to $1/\boldsymbol{r}^3$ away from the sample. From this consideration several conclusions can be made: (*i*) The near field coupling level is proportional to the inverse sixth power of the distance, $\sim 1/\boldsymbol{r}^6$ in the quasi-static near field zone; (*ii*) for a thin dielectric (moderate permittivity) object located in free space (without the substrate) the near field coupling strength is almost linearly proportional (at the same imaging distance) to the strip thickness and its dielectric permittivity ε_1; (*iii*) in the presence of the substrate, the near field coupling depends on the sum of polarization currents $J_{1y}(\boldsymbol{r}_1) + J_{2y}(\boldsymbol{r}_2)$ and therefore the thin strip resolution contrast depends on the ratio between the dielectric permittivities ε_1 and ε_2. For the situation when $|\varepsilon_2| >> |\varepsilon_1|$ the resolution contrast may sufficiently deteriorate with thickness *d* reduction. To illustrate this analysis two imaging experiments involving very thin PVC dielectric film (ε_1 =3) strips have been carried out. In the first experiment, four films of various thicknesses have been positioned on the 1cm thick Rohacell

foam substrate with relative permittivity ε_{foam} =1.07. The strips length are 35mm, widths are 10mm. The thickness varies from d=50μm, (first strip), 2d (second strip), 3d and 5d for the third and fourth strips correspondingly, Fig.10(a). In terms of a wavelength at 4GHz, d=λ/1500.

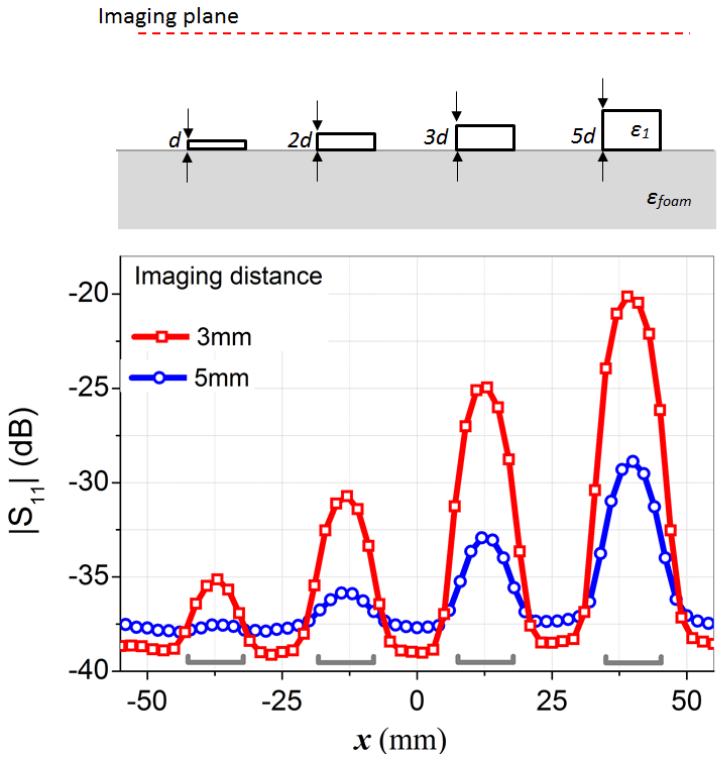

(a)

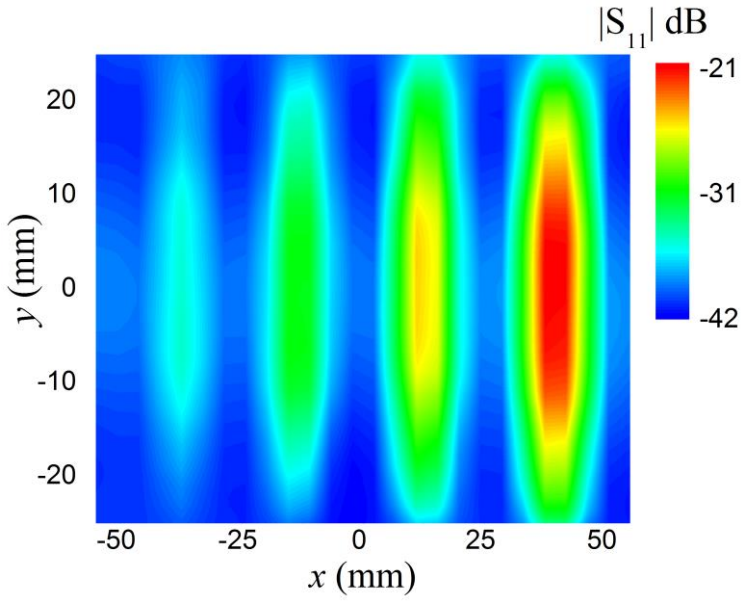

(b)

Fig. 10. Amplitude reflection image of four dielectric strips on a foam substrate. (a) *x* cut; (b) *xy* plane, imaging distance 3mm. Grey markers show the position of the strips along the x range in Fig.10(a).

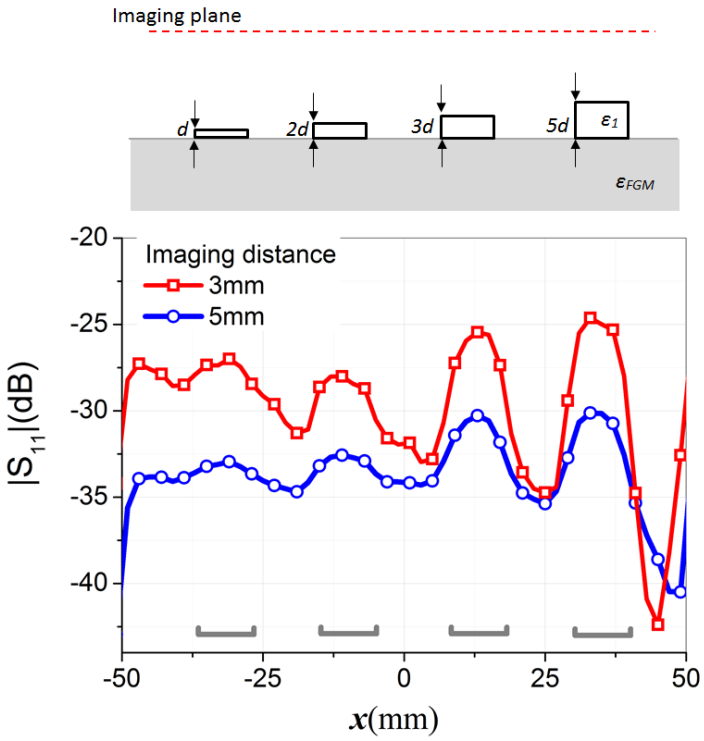

Fig. 11. Amplitude reflection image of four dielectric strips on a FGM dielectric substrate in *x* cut (y=0).

Fig. 10(a) shows the reflection image of the sample in the x cut (y=0) for two imaging distances, 3mm and 5mm. It can be seen that at 3mm distance the amplitude resolution contrast between the first and second strips is around 5dB (phase contrast more than 15 degrees) therefore in the considered low permittivity substrate scenario the thickness resolution of order 10^{-3} λ can be achieved.

In the second experiment the strips were positioned on the 1mm thick FGM-U-40 lossy dielectric sheet with real part of the permittivity $\mathrm{Re}(\varepsilon_{FGM})\sim 10$, loss tangent $\tan\delta\sim 0.3$. The amplitude reflection image shown in Fig. 11 shows that in the situation when the permittivity of the substrate is much higher than the permittivity of a thin strip accurate discrimination of the strips of the considered thickness (10^{-3} λ) is not possible. It is worthy to note, however that the strips are clearly resolved from the substrate with amplitude contrast 5dB-10dB at 3mm imaging distance.

7. Comparison between the loaded aperture probe and open-ended coaxial probe

In this Section we compare the near field focusing and microwave energy transmission properties of the proposed folded strip loaded aperture probe with those of an open-ended coaxial probe widely used for biomedical imaging and dielectrics characterization [2], [7]-[11].

Fig.12 shows the comparison between the open-ended coaxial and loaded slot aperture probes. In Fig.12(a) a full width at half-maximum (FWHM) of the near *E*-field pattern has been calculated using FEKO solver (www.feko.info) for the loaded aperture used in this paper and a coaxial cable probe based on the standard RG-402 coaxial cable with 3mm outer diameter, 0.9mm inner cable diameter and 3mm tip length. It can be seen from Fig.12(a) that the proposed loaded aperture probe has the same FWHM (in one of the dual hot spots) as a coaxial cable at short imaging distances ($|z|<0.05\lambda$). At larger imaging distances, $|z|>0.05\lambda$ the FWHM of the coaxial cable grows faster than the FWHM of the loaded probe thus the loaded aperture probe can operate at much larger imaging distances with better spatial resolution.

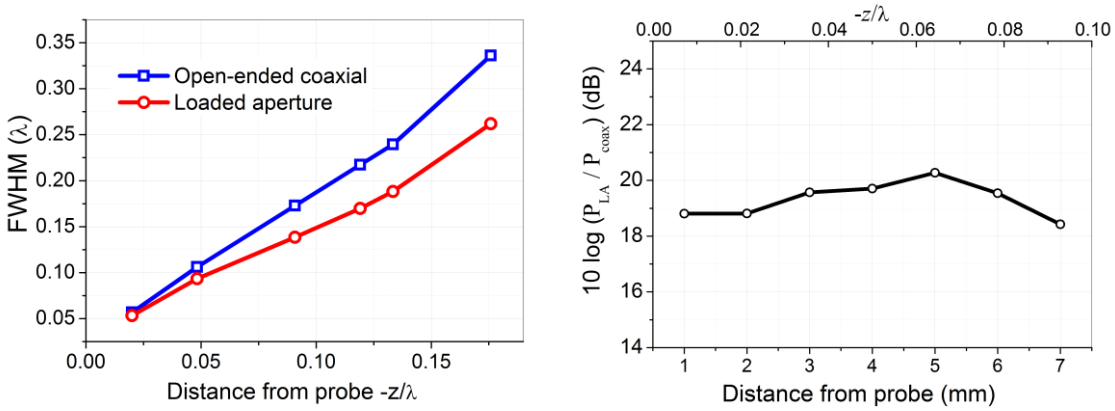

(a) (b)

Fig. 12. FWHM vs the stand-off distance (a) and measured at 4GHz relative transmitted power of the loaded aperture probe and the open-ended coaxial probe as a function of the standoff distance (b).

Another important advantage of the loaded aperture probe is its ability to efficiently transmit microwave energy at the S_{11} resonance unlike the open-ended coaxial probe which radiates only a very small (~1%) part of the input microwave power [7]. This property of the loaded aperture probe could be very useful in microwave hyperthermia applications. Also by virtue of this property the loaded aperture probe can operate at very small levels of microwave power without significant loss of sensitivity. The measured relative microwave transmitted power, $10\log(P_{LA}/P_{coax})$ as a function of stand-off distance from the probes is shown in Fig. 12(b). In this graph P_{LA} and P_{coax} are the power densities integrated across the respective focal spot areas of the loaded probe and the open-ended coaxial at -6dB level. The transmitted power is obtained by using a small monopole antenna with 5mm arms collecting all three polarizations of the electric field. A source input power level of 0dBm has been used for the excitation of both the loaded aperture and open-ended coaxial probes. It is important to note that the loaded aperture probe can deliver 20dB more power to the focal spot than the open-ended coaxial probe for the same source input power level.

8. Conclusions

A novel type of microwave probes based on the loaded aperture geometry has been proposed and experimentally evaluated for dielectric characterization and near field imaging with deep subwavelength resolution. It has been shown that the probe can resolve thin lossy dielectric samples with very high contrast (~10dB) and spatial accuracy (better than $\lambda/10$) over a wide range of standoff distances in the near field zone (0.02λ–0.2λ). High sensitivity of the proposed loaded aperture probe to biological materials containing water has been demonstrated. Particularly it has been shown that the probe can image wet and dry leaves with extremely high amplitude (~20dB) and phase (~100 degrees) contrast and spatial resolution (better than 5mm at 4GHz). A microwave imaging scenario for the early-stage skin cancer identification based on the artificial dielectric model has also been explored. This model study shows that the typical resolution of an artificial malignant tumour with

a characteristic size of one tenth of a wavelength can be discriminated with at least 6dB amplitude and 50 degrees phase contrast from the artificial healthy skin and with more than 3dB contrast from a benign lesion of the same size. The near field focussing properties of the proposed imaging device when compared to those of a standard open-ended coaxial probe are found to be superior in terms of focussed microwave power transmission and low-level power sensing applications.

Acknowledgment

The authors thank the anonymous reviewers for valuable and insightful comments and suggestions allowed to improve the original manuscript.

References

[1] Vander Vorst A, Rosen A, Kotsuka Y.: "RF/Microwave Interaction with Biological Tissues", 2006, John Wiley & Sons

[2] Brace C.: "Thermal tumor ablation in clinical use", IEEE Pulse **,** 2011, 2**,** (5), pp. 28-38 http://ieeexplore.ieee.org/stamp/stamp.jsp?tp=&arnumber=6042585

[3] Cavagnaro M et al.: "A minimally invasive antenna for microwave ablation therapies: design, performances, and experimental assessment", IEEE Trans Biomed. Eng. 2011, 58, (4), pp. 949-959 http://ieeexplore.ieee.org/stamp/stamp.jsp?tp=&arnumber=5668498

[4] Hung-Wei Chiu et al.: "Pain control on demand based on pulsed radio-frequency stimulation of the dorsal root ganglion using a batteryless implantable CMOS SoC", IEEE Trans Biomed. Circuits Systems, 2010, 4, (6) 350-359 http://ieeexplore.ieee.org/stamp/stamp.jsp?tp=&arnumber=5634138

[5]Caratelli D. et al.: "Accurate time-domain modeling of reconfigurable antenna sensors for non-invasive melanoma skin cancer detection", IEEE Sensors Journal , 2012,12, (3) pp. 635-643 http://ieeexplore.ieee.org/stamp/stamp.jsp?arnumber=5716652

[6] Korostynska O.: "Glucose monitoring using electromagnetic waves and microsensor with interdigitated electrodes", IEEE Sensors Applications Symp 2009, 34-37, DOI 10.1109/SAS.2009.4801772 http://ieeexplore.ieee.org/stamp/stamp.jsp?tp=&arnumber=4801772

[7] McLaughlin B., Robertson P.: "Submillimeter coaxial probes for dielectric spectroscopy of liquids and biological materials", IEEE Trans. Microwave Theory Techniques, 2009, 57, (12), pp. 3000-3010 http://ieeexplore.ieee.org/stamp/stamp.jsp?tp=&arnumber=5335467

[8] Athey T., W, Stuchly M., Stuchly S.: "Measurement of radio frequency permittivity of biological tissues with an open-ended coaxial line: Part I", IEEE Trans. Microwave Theory Techniques 1982, 30, (1), pp. 82-86 http://ieeexplore.ieee.org/stamp/stamp.jsp?tp=&arnumber=1131021

[9] Hagl D. et al.: "Sensing volume of open-ended coaxial probes for dielectric characterization of breast tissue at microwave frequencies", IEEE Trans. Microwave Theory Techniques, 2003, 51, (4), pp. 1194-1206 http://ieeexplore.ieee.org/stamp/stamp.jsp?tp=&arnumber=1220119

[10] Obol M., Al-Moayed N., Naber S. P., Afsar M. N.: "Using coaxial probe for broadband microwave characterization of biological tissues", 38th European Microwave Conference, 2008, pp. 416-419 DOI 10.1109/EUMC.2008.4751477 http://ieeexplore.ieee.org/stamp/stamp.jsp?tp=&arnumber=4751477

[11] Peng Wang, Brace C.: "Tissue dielectric measurement using an interstitial dipole antenna", IEEE Trans. Biomed. Eng., 2012, 59 (1), pp. 115-121 http://ieeexplore.ieee.org/stamp/stamp.jsp?tp=&arnumber=6016214

[12] Seaman R., Burdette E., Dehaan R.: "Open-ended coaxial exposure device for applying RF/microwave fields to very small biological preparations", IEEE Trans. Microwave Theory Techniques, 1989, 37, (1), pp. 102-110 http://ieeexplore.ieee.org/stamp/stamp.jsp?tp=&arnumber=20028

[13] Byoungjoong Kang et al.: "Novel low-cost planar probes with broadside apertures for nondestructive dielectric measurement of biological materials at microwave frequencies", IEEE Trans. Microwave Theory Techniques, 2005, 53, (1), pp. 134-143 http://ieeexplore.ieee.org/stamp/stamp.jsp?tp=&arnumber=1381683

[14] Dalmay C., et al.: "Microwave sensors for stem cell identification and discrimination", 2010 IEEE Microwave Symposium Digest 2010, pp. 620-623 DOI 10.1109/MWSYM.2010.5514663

[15] Smith G.: "The electric-field probe near a material interface with application to the probing of fields in biological bodies", IEEE Trans. Microwave Theory Techniques, 1979, 27, (3), pp. 270-278 http://ieeexplore.ieee.org/stamp/stamp.jsp?tp=&arnumber=1129606

[16] Courtney C. , Motil W.: "One-port time-domain measurement of the approximate permittivity and permeability of materials", IEEE Trans. Microwave Theory Techniques 1999, 47, (5), pp. 551-555 http://ieeexplore.ieee.org/stamp/stamp.jsp?tp=&arnumber=763154

[17] Sarabandi K., Ulaby F.: "Technique for measuring the dielectric constant of thin materials", IEEE Trans Instrumentation and Measurement", 1988, 37, (4), pp. 631-636 http://ieeexplore.ieee.org/stamp/stamp.jsp?tp=&arnumber=9828

[18] Pochiraju T., Malyuskin O., Fusco V.: "Sub-wavelength near field imaging using a non-resonant slot with a wire insert", IEEE Antennas Propagat Int Symp. 2010, pp.1-4, DOI 10.1109/APS.2010.5561655

[19] Pochiraju T., Malyuskin O., Fusco V.: "Tunable near-field subwavelength microwave imaging", Microwave and Optical Technology Letters, 2011, 53, (6), pp. 1229-1231 DOI: 10.1002/mop.25966 http://onlinelibrary.wiley.com/doi/10.1002/mop.25966/pdf

[20] Malyuskin O., Fusco V.: "Near field enhancement and subwavelength imaging using resonantly loaded apertures", IEEE Trans. Antennas and Propagation, 2014, 62, (6), pp. 3130-3140 DOI: 10.1109/TAP.2014.2314488 http://ieeexplore.ieee.org/stamp/stamp.jsp?tp=&arnumber=6781014

[21] Taeb A., Gigoyan S, Safavi-Naeini, S.: "Millimetre-wave waveguide reflectometers for early detection of skin cancer", IET Microw. Antennas Propag., vol. 7, no. 14, pp. 1182–1186, 2013.

[22] Mehta P. et al.: "Microwave reflectometry as a novel diagnostic tool for detection of skin cancers", IEEE Trans. Instrumentation Measurements, vol. 55, no 4, pp. 1309-1316, Aug. 2006.

[23] Suntzeff V. and Carruthers C.: "The water content in the epidermis of mice undergoing carcinogenesis by methylcholanthrene," Cancer Research, vol. 6, pp. 574–577, 1946.

[24] Gniadecka, M. et al:, "Melanoma diagnosis by Raman spectroscopy and neural networks: Structure alterations in proteins and lipids in intact cancer tissue," J. Invest. Dermatol., vol. 122, no. 2, p. 443, Feb. 2004.

[25] Emerson and Cuming Microwave Products, Inc. http://eccosorb.eu/products/eccosorb

[26] Pozar, D., "Microwave Engineering", 2012, John Wiley & Sons

[27] Gao, J.: "Analytical formulas for the resonant frequency changes due to opening apertures on cavity walls", Nuclear Instruments and Methods in Physics Research Section A: Accelerators, Spectrometers, Detectors and Associated Equipment, vol. 311, no. 3, 1992, pp. 437–443.

[28] Obol, M, Al-Moayed, N. Ayala, A.M, Afsar, M.: "Wireless Sensor Using High Q Resonator of Single Walled Carbon Nanotube for Liquids", 38th European Microwave Conference EuMC 2008, pp. 1185 – 1188, 27-31 Oct. 2008.

[29] http://www.nearfield.com/products/PlanarSystemsIndex.aspx

[30] Gabriel S., Lau R W and Gabriel C.: "The dielectric properties of biological tissues: II. Measurements in the frequency range 10 Hz to 20", Phys. Med. Biol., vol. 41, pp. 2251–2269, 1996.

[31] Gabriel S., Lau R W and Gabriel C.: "The dielectric properties of biological tissues: III. Parametric models for the dielectric spectrum of tissues", Phys. Med. Biol., vol. 41, pp. 2271–2293, 1996.

[32] www.cancerresearchuk.org , http://www.skincancer.org/melanoma

[33] Landau, L.D., Pitaevskii, L. P., Lifshitz , E.M.: "Electrodynamics of Continuous Media", Elsevier, Oxford, UK, 1984.